



HAL
open science

Equation of state and CaCl transformation of Al-bearing silica up to 100 GPa and 3000 K

Nathalie Bolfan-Casanova, Denis Andrault, E. Amiguet, N. Guignot

► **To cite this version:**

Nathalie Bolfan-Casanova, Denis Andrault, E. Amiguet, N. Guignot. Equation of state and CaCl transformation of Al-bearing silica up to 100 GPa and 3000 K. *Physics of the Earth and Planetary Interiors*, 2009, 174 (1-4), pp.70. 10.1016/j.pepi.2008.06.024 . hal-00533032

HAL Id: hal-00533032

<https://hal.science/hal-00533032>

Submitted on 5 Nov 2010

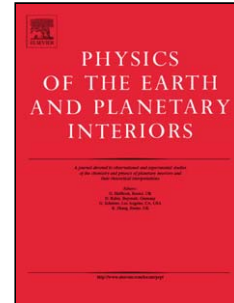
HAL is a multi-disciplinary open access archive for the deposit and dissemination of scientific research documents, whether they are published or not. The documents may come from teaching and research institutions in France or abroad, or from public or private research centers.

L'archive ouverte pluridisciplinaire **HAL**, est destinée au dépôt et à la diffusion de documents scientifiques de niveau recherche, publiés ou non, émanant des établissements d'enseignement et de recherche français ou étrangers, des laboratoires publics ou privés.

Accepted Manuscript

Title: Equation of state and CaCl_2 transformation of Al-bearing silica up to 100 GPa and 3000 K

Authors: N. Bolfan-Casanova, D. Andrault, E. Amiguet, N. Guignot



PII: S0031-9201(08)00154-4
DOI: doi:10.1016/j.pepi.2008.06.024
Reference: PEPI 4985

To appear in: *Physics of the Earth and Planetary Interiors*

Received date: 15-10-2007
Revised date: 26-5-2008
Accepted date: 30-6-2008

Please cite this article as: Bolfan-Casanova, N., Andrault, D., Amiguet, E., Guignot, N., Equation of state and CaCl_2 transformation of Al-bearing silica up to 100 GPa and 3000 K, *Physics of the Earth and Planetary Interiors* (2007), doi:10.1016/j.pepi.2008.06.024

This is a PDF file of an unedited manuscript that has been accepted for publication. As a service to our customers we are providing this early version of the manuscript. The manuscript will undergo copyediting, typesetting, and review of the resulting proof before it is published in its final form. Please note that during the production process errors may be discovered which could affect the content, and all legal disclaimers that apply to the journal pertain.

1 **Equation of state and CaCl₂ transformation of**
2 **Al-bearing silica up to 100 GPa and 3000 K**

3 N. Bolfan-Casanova ^{1*}, D. Andrault ¹, E. Amiguet ^{1,2}, and N. Guignot ³

4 ¹ Laboratoire Magmas et Volcans, Université B. Pascal, Clermont-Ferrand, France

5 ² now at Laboratoire de Structure et Propriétés de l'Etat Solide, Lille, France

6 ³ SOLEIL-synchrotron, Gif-sur-Yvette, France

7
8 **Abstract**

9 Structure and density of the Al-bearing silica phases were investigated at high pressure and
10 temperature by means of powder X-ray diffraction in laser heated diamond anvil cell at the
11 ID30 beamline of the ESRF. The transition from rutile (TiO₂) to calcium chloride (CaCl₂)
12 phase occurs at lower pressure, down to 23 GPa at 300 Kelvin, compared to 50 GPa in the
13 pure SiO₂ system. The distortion increases with pressure and decreases with temperature. We
14 determined experimentally the clapeyron slope of the transition: dP/dT of 0.02 GPa/K.
15 According to the phase diagram determined by *in-situ* X-ray diffraction, Al-bearing silica
16 should be in the CaCl₂ form in most of the transition zone and lower mantle. Also, aluminous
17 silica, whether in the rutile or calcium chloride form, is softer than pure silica. Our results
18 show that the incorporation of ~2.3 weight % of alumina in silica decreases its bulk modulus
19 of around 7-10% in case of the rutile form and of 3.5 % in case of the CaCl₂ form.

20 **Keywords: stishovite, CaCl₂, aluminum, phase transition, Clapeyron slope**

21 * Corresponding author: Nathalie Bolfan-Casanova

22 Laboratoire Magmas et Volcans, 5 rue Kessler, 63000 Clermont-Ferrand

23 Fax : 00 + 33 4 73 34 67 44

24 N.Bolfan@opgc.univ-bpclermont.fr

25

26 **Introduction**

27 Since seismic tomography images have shown slabs entering the lower mantle,
28 comprised between 670 and 2900 km depth (van der Hilst et al., 1997), the recycling of
29 oceanic crust into the deep Earth offers a way of enriching the mantle in silica. Indeed,
30 experimental petrology studies indicate that in subduction zones stishovite (tetragonal rutile
31 structure $P4_2/mnm$) crystallises above 9 GPa in the basaltic and sedimentary portions of the
32 subducted oceanic crust. Stishovite becomes more and more abundant as a result of the
33 dissolution of clinopyroxene into garnet structure (Irifune and Ringwood, 1987). Also,
34 stishovite has been shown to be an ubiquitous product of dehydration reactions occurring in
35 sedimentary and basaltic wet compositions (Ono, 1998). In such a subduction context
36 stishovite could contain up to 9 weight percent Al_2O_3 (Ono, 1999)(Ono, 1998). The
37 incorporation of even small amounts of this element and its possible coupling with oxygen
38 vacancies, following the reaction $Si^{4+} = Al^{3+} + \frac{1}{2} \square_O^{2+}$, can influence the stability, density and
39 the compressibility of mantle phases. Such parameters are important in the assessment of the
40 density, composition and thermal structure of the deep mantle.

41 In addition, pure stishovite undergoes a displacive phase transition to orthorhombic
42 $CaCl_2$ structure ($Pnmm$ space group) at pressure around 50 GPa, as demonstrated by several
43 experiments using either X-ray diffraction (Andrault et al., 1998a; Hemley et al., 2000;
44 Kingma et al., 1996; Tsuchida and Yagi, 1989) or Raman spectroscopy (Hemley et al., 2000;
45 Kingma et al., 1995). The onset of the phase transformation was reported between ~45 and
46 ~60 GPa by the different authors. Here, we present the first structural evidence on the effect
47 of aluminium on the transition of rutile to $CaCl_2$ structure of silica *in-situ* at high-pressure and
48 high-temperature using the laser-heated diamond anvil cell technique up to ~100 GPa and
49 more than 3000 K.

50

51 **Experimental procedure**

52 Two different types of aluminous silica containing around 4 wt% Al_2O_3 were used as starting
53 material. One of them is a glass, loaded without any grinding. Due to its treatment at very
54 high temperature and small surface/volume ratio of the sample, it should contain a negligible
55 amount of water. This sample is ideal for heating using CO_2 laser. However, in order to heat
56 with a YAG laser and to be able to measure pressure at high-temperature we had to mix the
57 sample with a laser absorber such as platinum. Thus, a gel of the same composition was
58 prepared in order to be mechanically mixed with Pt powder.

59 We performed experiments at different pressure and temperature conditions (see
60 **Table 1**). To generate high pressures, we used a membrane-type diamond anvil cell equipped
61 with 300- μm diamond culets. Re-gaskets were pre-indented to 40-50 μm thickness before
62 drilling a 80- μm hole using electro-erosion. Samples were loaded together with a small ruby
63 chip and the pressure medium. Ar pressure medium (loaded cryogenically) was used in CO_2 -
64 laser heating experiments whereas NaCl pressure medium was preferred for YAG-laser
65 heating experiments, still Ar was sometimes used. Laser-heating was used to synthesize
66 stishovite or post-stishovite *in-situ* in the DAC, and to release the deviatoric stresses after
67 each pressure increase. The setup is composed of two 40 W single-mode continuous YAG
68 lasers with excellent power stability focused on each side of the sample. The X-ray beam
69 intensity on ID30 was sufficient to obtain high quality angle-dispersive diffraction patterns in
70 60 s, which further minimizes any potential temperature deviation to a few tens of K. We
71 measured temperature on one side of the sample by the spectroradiometric method using
72 reflective collecting optics. Temperature were measured three times during collection of X-
73 ray diffractograms and the temperature variation was within 50 degrees in average, except

74 above 2200K where it reached 100 degrees due to melting of the pressure medium Ar or
75 NaCl.

76 For decompression measurements in Argon, no annealing was performed in order to
77 avoid to revert into the low-pressure phase. As a consequence of such decompression
78 measurements the pressure derivative of the bulk modulus cannot be derived with a good
79 degree of accuracy.

80 The X-ray diffraction patterns were collected *in-situ* at high pressure at the ID30
81 beamline of the European Synchrotron Radiation Facility (ESRF) using angle dispersive
82 radiation (Andrault and Fiquet, 2001; Mezouar et al., 2005; Schultz et al., 2005). A channel-
83 cut, water-cooled monochromator was used to produce a bright monochromatic X-ray beam
84 at 0.3738 Å wavelength. Vertical and horizontal focusing was achieved by bent-silicon
85 mirrors, the curvatures of which were adapted to obtain an optimal X-ray flux on a full width
86 at half maximum of less than 10x10 µm spot on the sample. Two-dimensional images were
87 recorded on an image plate and integrated using the Fit2d code (Hammersley, 1996). All X-
88 ray spectra were treated using the Rietveld method with the GSAS package (Larson and Von
89 Dreele, 1988).

90 Both Ar, ruby, and/or Pt pressure standards were available in our pressure chamber.
91 Ruby was mainly used to reach the target pressure for first synthesis. We preferred the
92 pressure provided by the Ar or Pt equation of state (EoS) (Holmes et al., 1989; Jamieson et
93 al., 1982; Jephcoat, 1998), because it can be recorded at the same position as the sample, and
94 therefore the potential artefacts related to pressure gradient in the sample chamber are
95 discarded. At high temperature, we used the Pt EoS (Jamieson et al., 1982) to derive the
96 pressure in the hot sample that can be affected by the effect of thermal pressure (Andrault et
97 al., 1998b). The error of volume measurement at the ID30 beamline was of about $2 \cdot 10^{-4}$. At

98 30 GPa pressure, it translates to pressure errors of ~ 0.3 or ~ 1 GPa, when using Ar or Pt
99 pressure standards, respectively.

100

101 **Experimental results**

102 a) Lattice distortion at room temperature

103 At high pressures, X-ray diffraction patterns display the presence of the pressure medium, Ar
104 or NaCl, Pt black if added, SiO_2 , and sometimes corundum (**Fig. 1**). The latter being due to an
105 excess of alumina in the starting composition compared to the Al solubility in silica under
106 some conditions of pressure and temperature. Looking closely at the diffraction patterns
107 recorded at lower pressure, it appears that the CaCl_2 -form appears at a pressure as low as
108 about 23 GPa at 300 K, as shown in **Figure 2a** by the splitting of the c/a and c/b parameter
109 ratios recorded at room temperature after laser annealing.

110 **Figure 3a** also shows the increase of the splitting of diffraction peaks with pressure at
111 298 K. Indeed, the rutile model of stishovite fails to explain spectral regions located at ~ 12 ,
112 14, and 17 degrees of the 2θ diffraction angle, where splitting of the $[120,210]$, $[121,211]$,
113 and $[130,310]$ lines is observed (see insets in **Fig. 1**). This clearly evidences the occurrence of
114 the orthorhombic ($Pnmm$) lattice of the CaCl_2 -form of SiO_2 at such low pressure. In **Figure**
115 **2a**, we also report previous results for Al-free stishovite (Andrault et al., 1998a) showing that
116 at 300 K the transition occurs at ~ 50 GPa. The comparison between Al-bearing and Al-free
117 samples raises three important points: first, the distortion appears at much lower pressure in
118 the Al-bearing SiO_2 system. Second, the distortion increases quite rapidly above the transition
119 pressure for the Al-free phase, while it is very progressive for the Al-bearing samples. Finally,
120 the distortion appears similar for both Al-free and Al-bearing compounds above 70 GPa.
121 Therefore, the most apparent effect of Al on the structure of stishovite is to facilitate the
122 CaCl_2 -distortion in the 23-70 GPa pressure range.

123 **Figure 2b** displays the distortion of aluminous silica samples synthesized at different
124 pressures and decompressed in Ar without annealing. In the case where the sample is
125 synthesized in the stability field of the rutile-form, e.g. stishovite, the decompression curves
126 display a normal, i.e. linear, behavior. Whereas, in the case where the sample is synthesized in
127 the stability field of the CaCl_2 form we observe a peculiar behavior during decompression. In
128 one case, the CaCl_2 structure of silica is conserved down to 10 GPa and then the sample
129 reverts to the rutile form. In the other case the CaCl_2 form was quenched to room pressure.

130 However, in the laser-annealed experiments we did not detect any systematic difference
131 in cell parameters due to a change in starting material from glass to gel nor from a change in
132 laser from CO_2 to YAG.

133

134 b) Lattice distortion at high temperature

135 For nominal pressures (at 300K) of 23, 26, and 36 GPa, we clearly observe a decrease of the
136 CaCl_2 cell distortion as a function of increasing temperature (**Fig. 3b** and **Fig. 4**). Because of
137 thermal pressure, the pressure increases with increasing temperature (Andrault et al., 1998b),
138 and the thermal pressures measured in this study thanks to the Pt scale (Jamieson et al., 1982)
139 agree with those calculated from an average bulk modulus of 290 GPa for aluminous silica
140 and an expansion coefficient of $1.6 \times 10^{-5} \text{ K}^{-1}$ as measured for pure stishovite (Nishihara et al.,
141 2005). Thus, we find that the rutile structure appears around 2230 K at 20.3 GPa, 2934 K at
142 35.0 GPa and potentially ~ 3500 K at 49 GPa, if we extrapolate the c/a and c/b ratios of
143 **Figure 4** using the pressure-temperature relationship measured in this study using Pt. This
144 clearly evidences a positive Clapeyron slope for the transition from rutile to CaCl_2
145 polymorphs of Al-bearing silica (see discussion).

146

147 **Discussion**

148

149 a) Al incorporation in rutile and CaCl₂ phases of silica150 The volumes of the aluminous silica phases (rutile or CaCl₂ structure) measured at room151 pressure are significantly higher than that of pure stishovite (see **Figure 5**). In our study all

152 samples were quenched to room pressure under the form of stishovite except for one sample,

153 Alsti-06, that was quenched in the form of post-stishovite. In **Figure 5** the correlation154 between the volume of Al-bearing stishovite and its Al content is $V_0(\text{\AA}^3) = 46.517 + 12.461 \times$ 155 X_{Al} (Al p.f.u.) as retrieved by Lakshtanov et al. (2005; 2007) based on multi-anvil samples.

156 We used this relationship to interpolate the Al content of the silica phases synthesized in this

157 study knowing their ambient pressure volume. One limitation of this method for determining

158 the Al content could be that our silica phases were synthesized under dry conditions whereas

159 the correlation is built from the volume of stishovite synthesized under wet conditions (except

160 for pure stishovite). Still, (Litasov et al., 2007) have shown that only one seventh of Al

161 incorporated into stishovite is associated with H. It is thus expected that hydration has a small

162 effect on the correlation of cell volume and Al content. Using this correlation, we calculate

163 that our samples (only those quenched under the rutile form) contain between 2.2 and 3.6

164 wt% Al₂O₃, or an average Al content of 2.9 ± 0.6 wt% Al₂O₃. This variation is explained by

165 the fact that solubility of Al in silica is not that high. It is thus difficult to avoid changes in

166 concentration due to overstepping the solubility limit when different pressure conditions are

167 used together with laser annealing. The sample quenched under the form of CaCl₂ displays a168 very large volume of 47.773\AA^3 (see **Table 1**), which leads to an Al content in the phase (0.1

169 Al per formula unit) that is anomalously large given that the starting material only contains

170 0.047 Al p.f.u (4 wt% Al₂O₃). The fact that this sample falls off the trend can be explained by

171 its structural difference with stishovite.

172 Still, a systematic study of the effect of pressure and temperature on the solubility of
173 Al_2O_3 in both the rutile and CaCl_2 stability field of silica is lacking. Ono (1999) reports that in
174 the Al_2O_3 - SiO_2 - H_2O system the Al content in stishovite increases with temperature up to 9
175 wt% at 20 GPa and 1700°C. However, in the dry system incorporation of aluminum into silica
176 seems to be much more limited. In the Al_2O_3 - SiO_2 , kyanite, composition (Liu et al., 2006)
177 find that solubility increases with temperature up to 2.5 wt% Al_2O_3 at 2000°C then decreases,
178 at least up to pressures of 22 GPa. This maximum Al content is consistent with the values for
179 two samples synthesized here at 16.7 and 23.7 GPa for which the correlation between cell
180 volume and Al content yields 2.2 and 2.4 wt% Al_2O_3 , respectively. They also report that
181 solubility of Al_2O_3 decreases with increasing pressure which is contradictory to our
182 observation. But note that the observation of (Liu et al., 2006) that Al solubility decreases
183 with increasing temperature is valid only until 22 GPa. Thus the information is lacking for the
184 solubility of Al in the silica phase within the stability field of the CaCl_2 phase of silica, *i.e.*
185 above 23 GPa, which represents the case of our most aluminous samples. In addition, (Ono et
186 al., 2001b) report that at 30 GPa in the MORB composition, Al content in stishovite (as
187 recovered at room pressure) reaches 4.2 wt% Al_2O_3 , thus indicating a different behavior from
188 the results of (Liu et al., 2006) at high pressures within the stability field of the CaCl_2 phase.
189 The difference could be due either to the presence of water or to intrinsically different
190 solubility of Al in rutile or CaCl_2 structure.

191

192 b) Lattice strain

193 (Kingma et al., 1995) evidenced the softening of the B_{1g} rutile mode in pure SiO_2 using
194 Raman spectroscopy with neon pressure medium up to 60 GPa. They observed the transition
195 from tetragonal to orthorhombic structure at 50 GPa and that it is reversible. They concluded
196 to a second order phase transition. (Andrault et al., 1998a) observed the transition at 54 GPa

197 using powder X-ray diffraction, without any pressure medium but with laser-annealing, and
198 did not observe any substantial discontinuity in volume, suggesting that the transition has
199 mainly a second order character. Still, they noted a sudden increase of distortion of the
200 tetragonal lattice just above the transition pressure, which could indicate a certain degree of
201 first-order character of the transition. (Hemley et al., 2000) performed reversal compression
202 experiments using X-ray single crystal diffraction and Raman spectroscopy in hydrogen
203 pressure medium. They observed the transition to CaCl_2 structure at 58 GPa but also observed
204 an hysteresis on decompression and CaCl_2 remaining down to 40 GPa. This provides another
205 argument for a weak first-order character of the transition.

206 In this study, we observe that the incorporation of Al in silica promotes the transition
207 from rutile to CaCl_2 at very low pressures, down to 23 GPa. If one compares the transition
208 pressure found in the different studies on pure SiO_2 , the effect of the pressure media (only 8
209 GPa, see references above) is clearly not enough to explain the lowering of the transition to
210 23 GPa. Thus, the lowering of the transition pressure is due to the presence of aluminum and
211 not to stress. Indeed, because Al^{3+} is larger than Si^{4+} , incorporation of aluminum induces a
212 chemical pressure that destabilizes the low-pressure polymorph, thus shifting the transition to
213 lower pressure. Very recently, (Lakshtanov et al., 2007b) have observed the CaCl_2 phase of
214 silica containing 5 wt% Al_2O_3 at 24.3 GPa at room temperature. Our results are identical to
215 theirs within experimental uncertainty, especially Al content. We find that the transition
216 occurs at pressures between 19 and 23 GPa for a maximum Al content of 4 wt% Al_2O_3 .

217 The interesting point is that a second order character provides the formalism to
218 calculate thermodynamic parameters, especially the entropy change associated with such
219 progressive transition. In such case, we can define an order parameter that represents the
220 degree of lattice strain. For small strains, the order parameter is $Q=(a-b)/a$ (Andrault et al.,
221 1998a; Carpenter et al., 2000). The order parameter shows lattice strain above ~ 23 GPa at 300

222 K in annealed samples (**Figure 6**). In this figure (a) it is confirmed that the distortion appears
223 above ~ 23 GPa for the Al-bearing stishovite, (b) the change with pressure of order parameter
224 $[d(Q^2)/dP]$ is found similar for Al-free and Al-bearing stishovite and (c) the abrupt change of
225 order parameter $[\Delta S]$ appears negligible for Al-bearing stishovite while it is clearly visible for
226 the Al-free phase.

227

228 c) Equation of state at 300 K

229 **Figure 7** displays the volumes at 300 K for the different samples measured during
230 compression+annealing or during decompression to room pressure. All aluminous silica
231 phases display higher volumes due to the fact that Al incorporation expands the unit-cell of
232 silica. On the other hand, the volume of aluminous silica tends to converge at high pressure,
233 with lower V/V_0 for Al-bearing stishovite compared to pure silica (except PV20). Firstly, if
234 we consider the range of pressure where the stishovite structure is stable, for example for
235 decompression curves of aluminous stishovite (Alsti-01 and Alsti-07), we observe that the Al-
236 bearing stishovite is clearly more compressible than pure stishovite with bulk modulus of
237 278 ± 4 GPa and 287 ± 5 GPa (for $K'=4.59$) or 284 ± 4 GPa and 291 ± 4 GPa (for $K'=4$),
238 depending on the pressure of synthesis or Al content (16.7 and 23.7 GPa, or 2.2 and 2.4 wt%
239 Al_2O_3 respectively), instead of $K_0=310 \pm 1$ GPa (for $K'=4.59$) or 324 GPa (for $K'=4$) for pure
240 stishovite (Andrault et al., 2003). These two Al-bearing stishovite samples have very similar
241 volumes and elastic behavior in agreement with their similar aluminum content.

242 Concerning the $CaCl_2$ -form, we report three P-V curves: one compression+annealing up
243 to 99.9 GPa (PV20) and two decompressions without annealing from 47.6 and 50.5 GPa
244 down to room pressure. Among these last two experiments one sample reverted to the rutile
245 structure without heating at ~ 10 GPa (PV21) whereas the other one retained its $CaCl_2$
246 structure down to ambient conditions (Alsti-06). The room pressure volume V_0 is thus

247 determined directly from the X-ray diffraction measurement or from extrapolation to 1 bar of
248 a second order Birch-Murnaghan EoS (**Table 1**). Compared to pure silica, aluminous silica
249 with CaCl₂ structure also displays higher volumes and lower V/V₀ than pure silica (Andrault
250 et al., 2003) (see **Figure 7**). The compression + annealing of aluminous silica up to 99.9 GPa
251 yields a K₀ of 322 ±7 GPa (for K'=4) or K₀ of 292 ±7 GPa (for K'₀=4.59). Compared to pure
252 CaCl₂ silica (K₀ of 334±7 GPa for K'=4, from (Andrault et al., 2003)) it appears that
253 aluminous silica with the CaCl₂ structure is slightly more compressible. The two
254 decompression experiments yield K₀ of 300 ±4 GPa (for K'=4) and K₀ of 259 ±3 GPa (for
255 K'=4) for PV21 and Alsti-06, respectively. The value for PV21 should be regarded with
256 caution because the sample changed structure in the course of the P-V measurement.

257 Thus, in this study we show that aluminium softens both the rutile and CaCl₂ phases of
258 silica. This softening is in agreement with expectations because K₀V₀ can be regarded as
259 almost constant. Concerning the rutile phase in comparison with pure silica, and using the
260 same K₀' of 4.59 determined by Andrault et al. (2003), the incorporation of an average of
261 ~2.3 weight % of alumina in stishovite decreases its bulk modulus of around 7-10%.
262 Concerning the CaCl₂ phase we also observe a decrease of bulk modulus of 3.5%.

263 Previous compressibility studies of aluminous silica have used P-V data sets that cross
264 the transition between the rutile to the CaCl₂ transition (Lakshtanov et al., 2005; Ono et al.,
265 2002). Thus the bulk moduli reported include compression behaviour of both the low and
266 high-pressure phases. (Ono et al., 2002) determined a K₀ of 282 GPa from 10 to 40 GPa
267 whereas (Lakshtanov et al., 2005) determined a K₀ of 304 GPa from 2 to 58 GPa, both using
268 second order Birch-Murnaghan Eos (K'=4), for samples containing 2.1 and 1.8 wt% Al₂O₃,
269 respectively. Our results indicate that the relationship K₀-V₀ is a function of the structure of
270 aluminous silica (see **Figure 8**). The two data points from (Lakshtanov et al., 2007a) display
271 much higher volume for the rutile phase containing both aluminum and hydrogen whereas the

272 bulk moduli are similar to stishovite measured in this study. There appears to be an additional
273 effect that may be related to the fact that these samples contain about 2400-2900 ppm by
274 weight of water (Lakshtanov et al., 2007a). It is clear that more data is needed to refine the
275 effect of Al content, water content and structure on the elasticity of aluminous silica at high-
276 pressure and temperature.

277

278 d) Phase diagram

279 As shown on **Figure 4** from the evolution of the cell parameter ratios we can see that the
280 orthorhombic distortion increases with pressure and decreases with temperature. **Figure 9**
281 shows all the experimental points from this study. The resulting clapeyron slope of the
282 transition is: dP/dT of 0.02 GPa/K. Such positive clapeyron slope of the transition is expected
283 for a pressure-induced order-disorder phase transformation (Andrault et al., 1998a; Ono et al.,
284 2001a). The rutile structure is stable at high temperature and low pressure while the calcium
285 chloride structure is stable at low temperature and high pressure. Comparing the transition
286 boundary with that of pure silica determined experimentally by (Ono et al., 2001a) clearly
287 shows that aluminum has a very large effect on the stability of the CaCl_2 form in the Earth's
288 mantle. In the presence of aluminum this phase can be found in most of the transition zone
289 and lower mantle. Of course, it is expected that the clapeyron slope of the transition depends
290 on Al content, but given that the $\text{SiO}_2 + 4 \text{ wt}\% \text{ Al}_2\text{O}_3$ system is close to saturation, the
291 transition boundary determined here should correspond to the lowest pressure one. As shown
292 in **Figure 5**, the Al content of the silica phases recovered under the rutile form at ambient
293 pressure varies between 2.2 and 3.6 wt% Al_2O_3 , due to synthesis of the samples at different
294 pressures. Since the system contained initially 4 wt% Al_2O_3 some corundum must have been
295 present in excess in the samples, but which was rarely detectable because of its low amount.
296 (Lakshtanov et al., 2007b) report the transition from rutile to CaCl_2 phase to take place

297 between 20.0 and 24.8 GPa at 300 K for an Al content of 6 wt% Al₂O₃. Such pressure is
298 extremely similar to that found in this study between 20 and 23 GPa but for an estimated Al
299 content of 3.1 wt% Al₂O₃.

300 Experimental petrology studies have shown that stishovite can incorporate substantial
301 Al contents, which are controlled by exchange with neighbouring phases such as
302 clinopyroxene or garnet. In sediment composition (Ono, 1998) has shown that Al content
303 increases with temperature at 15 GPa from 0.43 at 1100°C to 1.92 wt% Al₂O₃ at 1400°C. In
304 MORB composition, Al content ranges from 0.15 wt% Al₂O₃ at 18 GPa and 1000°C up to 4.2
305 % at 30 GPa an 1800°C (Litasov and Ohtani, 2005; Ono et al., 2001b). In our study the
306 ambient volumes of the different silica phases quenched from different pressures suggest a
307 variation in Al content from 2.2 to 3.6 wt% Al₂O₃. Thus values that are within the range of
308 those found in experiments on natural compositions.

309

310 **Conclusions**

311 In subducted slabs, a free SiO₂-phase is expected because the composition is much enriched
312 in incompatible elements. Since such elements comprise aluminum, the transition from
313 stishovite to the CaCl₂ phase will occur at lower pressures than in the Al-free system.
314 According to the phase diagram determined by *in-situ* X-ray diffraction, silica should be in
315 the CaCl₂ form in most of transition zone and lower mantle. Although we did not observe any
316 change in volume across the transition, the transformations show a high degree of hysteresis.
317 Thus, it is likely that the transition should not be connected with any density change, but it
318 can affect the seismic properties of descending slabs, because shear properties can be strongly
319 affected by such type of phase transformation (Carpenter et al., 2000; Lakshatanov et al.,
320 2007b).

321

322 **Acknowledgments**

323

324 The authors thank Y. Wang and E. Ohtani for editing this manuscript. Also two anonymous
325 reviewers greatly improved the quality by their comments.

326

Accepted Manuscript

327 **Figure captions:**

328

329 Figure 1: X-ray diffractogram recorded at 41 GPa and 300 K after laser heating at ~2500 K
330 using the gel starting composition. Diffraction peaks of Ar, Pt and the CaCl₂-form are clearly
331 visible. Small diffraction peaks (not indexed) correspond to minor amounts of corundum. A,
332 B, and C insets show selected two-theta regions where splitting of diffraction peaks evidence
333 the CaCl₂-distortion.

334

335 Figure 2: Evolution of the *c/a* and *c/b* cell parameter ratio of the silica structure as recorded at
336 300 K (a) on compression+annealing steps and (b) on decompression without annealing in Ar
337 pressure medium. Empty symbols represent the CaCl₂ structure, and full symbols the rutile
338 structure. Distortion is evidenced above ~23 GPa in Al-bearing system whereas for Al-free
339 silica the transition occurs around 50 GPa as reported previously (Andrault et al., 1998a). In
340 b) we can observe that the CaCl₂ can be quenched down to 10 GPa or even room pressure.

341

342 Figure 3: Evolution of the CaCl₂-distortion (a) with pressure at room temperature in Ar
343 pressure medium (experiment AlSti2 up to 49 GPa) and (b) with temperature at 23 GPa of
344 nominal pressure in NaCl pressure medium (experiment StiAl-01), for selected two-theta
345 zones.

346

347 Figure 4: Evolution with temperature of the *c/a* and *c/b* cell parameters ratio of aluminous
348 silica for three different nominal pressures (as measured at 300 K) for samples StiAl-01,
349 StiAl-02, StiAl-03 (see **Table 1**). Of course, the pressure is not constant at high-temperature

350 due to thermal pressure. The rutile structure appears around 2230 K at 20.3 GPa, 2934 K at
351 35.0 GPa and potentially ~3500 K at 49 GPa, if we extrapolate the c/a and c/b ratios.

352

353 Figure 5: Correlation between the room pressure volume of aluminous wet stishovite
354 synthesized in the multi-anvil press and its Al content. Previous data for pure stishovite are
355 from (Andrault et al., 2003), and for aluminous stishovite from (Smyth et al., 1995), (Ono et
356 al., 2002) and (Lakshtanov et al., 2005). Plotting the ambient cell volumes of the aluminous
357 silica phases synthesized in this study using DAC (circles) into this diagram allows to retrieve
358 their Al content. Empty symbols indicate samples that have been decompressed after one
359 single annealing, full symbols those which have experienced multiple pressures and
360 annealings. This figure suggests that the silica samples synthesized in this study (recovered
361 under the rutile form) contain between 2.2 and 3.6 wt% Al_2O_3 .

362

363 Figure 6: Evolution with pressure of the square of the order parameter $Q=(a-b)/a$ used to
364 quantify the lattice strain associated with the CaCl_2 distortion. Circles represent the
365 decompression in Ar pressure medium from 50.5 GPa, and squares the compression +
366 annealing in NaCl pressure medium up to 99 GPa. Also shown is the order parameter for pure
367 silica from Andrault et al. (2003) (diamonds). Although the cell parameters ratios of
368 aluminous silica show an hysteresis on decompression that would indicate a first order
369 character, there is no discontinuity on the order parameter across the transition. Also, the gap
370 observed for pure silica may be due to insufficient pressure resolution of the data coverage
371 rather than to a small degree of first order character.

372

373 Figure 7: P-V curves measured at 300 K for Al-bearing silica compounds shown as a function
374 of volume during compression+annealing and during decompression without annealing. Open
375 symbols represent the CaCl₂ structure and full symbols the rutile structure. Also shown is the
376 compression curve for pure silica from (Andrault et al., 2003).

377

378 Figure 8: Correlation between bulk modulus (for $K'=4$) and room pressure volume of
379 aluminous silica from this study and comparison with previous studies. The structure of the
380 phase is specified because in some cases the compression curve crossed the transition
381 between rutile to CaCl₂ phase. See text.

382

383 Figure 9: Phase diagram drawn for Al-bearing silica. Pressures at high temperature are
384 derived from volume measurements of the Pt pressure standard that is mixed with the sample.
385 The mantle geotherm is from (Katsura et al., 2004). Also shown as the dotted black curve is
386 the Clapeyron slope of the stishovite to post-stishovite phase transition in pure SiO₂ from
387 (Ono et al., 2001a). The phase boundary for aluminous stishovite can be expressed as dP/dT
388 of 0.02 GPa/K (green curve).

389 **References**

390

391 Andrault, D., Angel, R.J., Mosenfelder, J.L. and Le Bihan, T., 2003. Equation of state of the
392 stishovite to lower mantle pressures. *American Mineralogist*, 88: 301-307.393 Andrault, D. and Fiquet, G., 2001. Synchrotron radiation and laser-heating in a diamond anvil
394 cell. *Review of Scientific Instruments*, 72(2): 1283-1288.395 Andrault, D., Fiquet, G., Guyot, F. and Hanfland, M., 1998a. Pressure-induced Landau-type
396 transition in stishovite. *Science*, 23: 720-724.397 Andrault, D. et al., 1998b. Thermal pressure in a laser-heated diamond-anvil cell: An x-ray
398 diffraction study. *European Journal of Mineralogy*, 10: 931-940.399 Carpenter, M.A., Hemley, R.J. and Mao, H.K., 2000. High-pressure elasticity of stishovite
400 and the P4(2)/mnm reversible arrow Pnm phase transition. *Journal of Geophysical
401 Research*, 105(B5): 10807-10816.

402 Hammersley, J., 1996. Fit2d user manual, ESRF, Grenoble, France.

403 Hemley, R.J. et al., 2000. Solid/order parameter coupling in the ferroelastic transition in dense
404 SiO₂. *Solid State Communications*, 114(10): 527-532.405 Holmes, N.C., Moriarty, J.A., Gathers, G.R. and Nellis, W.J., 1989. Equations of state of
406 platinum to 660 GPa (6.6 Mbar). *Journal of Applied Physics*, 66: 2962-2967.407 Irifune, T. and Ringwood, A.E., 1987. Phase transformations in a harzburgite composition to
408 26 GPa: implications for dynamical behaviour of subducting slab. *Earth and Planetary
409 Science Letters*, 86: 365-376.410 Jamieson, J.C., Fritz, J.N. and Manghnani, M.H., 1982. Pressure measurement at high
411 temperature in x-ray diffraction studies: gold as a primary standard. In: S. Akimoto
412 and M.H. Manghnani (Editors), *High Pressure Research in Geophysics*. Riedel,
413 Boston, pp. 27-48.414 Jephcoat, A.P., 1998. Rare-gas solids in the Earth's deep interior. *Nature*, 393: 355-358.415 Katsura, T. et al., 2004. Olivine-wadsleyite transition in the system (Mg,Fe)₂SiO₄. *Journal of
416 Geophysical Research*, 109: doi:10.1029/2003JB002438.417 Kingma, K.J., Cohen, R.E., Hemley, R.J. and Mao, H.K., 1995. Transformation of stishovite
418 to a denser phase at lower mantle pressures. *Nature*, 374: 243-245.419 Kingma, K.J., Mao, H.K. and Hemley, R.J., 1996. Synchrotron x-ray diffraction of SiO₂ to
420 multimegabar pressures. *High Pressure Research*, 14: 363-374.421 Lakshatanov, D.L. et al., 2007a. Effect of Al³⁺ and H⁺ on the elastic properties of stishovite.
422 *American Mineralogist*, 92: 1026-1030.423 Lakshatanov, D.L. et al., 2007b. The post-stishovite phase transition in hydrous alumina-
424 bearing SiO₂ in the lower mantle of the Earth. *Proceedings of the National Academy
425 of Sciences of the USA*, 104: 13588-13590.426 Lakshatanov, D.L. et al., 2005. The equation of state of Al,H-bearing SiO₂ stishovite to 58
427 GPa. *Physics and Chemistry of Minerals*, 32(7): 466-470.

428 Larson, A.C. and Von Dreele, R.B., 1988. GSAS Manual, Los Alamos National Laboratory.

429 Litasov, K. et al., 2007. High hydrogen solubility in Al-rich stishovite and water transport in
430 the lower mantle. *Earth and Planetary Science Letters*, 262: 620-634.431 Litasov, K. and Ohtani, E., 2005. Phase relations in hydrous MORB at 18-28 GPa:
432 implications for heterogeneity of the lower mantle. *Physics of the Earth and Planetary
433 Interiors*, 150: 239-263.434 Liu, X. et al., 2006. Decomposition of kyanite and solubility of Al₂O₃ in stishovite at high
435 pressure and high temperature conditions, *Physics and Chemistry of Minerals*, pp.
436 711-721.

- 437 Mezouar, M. et al., 2005. Development of a new state-of-the-art beamline optimized for
438 monochromatic single-crystal and powder X-ray diffraction under extreme conditions
439 at the ESRF. *Journal of Synchrotron Radiation*, 12: 559-664.
- 440 Nishihara, Y., Nakayama, K., Takahashi, E., Iguchi, T. and Funakoshi, K., 2005. P-V-T
441 equation of state of stishovite to the mantle transition zone conditions. *Physics and*
442 *Chemistry of Minerals*: in press.
- 443 Ono, S., 1998. Stability limits of hydrous minerals in sediment and mid-ocean ridge basalt
444 compositions: Implications for water transport in subduction zones. *Journal of*
445 *Geophysical Research-Solid Earth*, 103(B8): 18253-18267.
- 446 Ono, S., 1999. High temperature stability limit of phase egg, $\text{AlSiO}_3(\text{OH})$. *Contribution in*
447 *Mineralogy and Petrology*, 137: 83-89.
- 448 Ono, S., Hirose, K., Murakami, M. and Isshiki, M., 2001a. Post-stishovite boundary in SiO_2
449 determined by in situ X-ray observations. *Earth and Planetary Science Letters*, in
450 press.
- 451 Ono, S., Ito, E. and Katsura, T., 2001b. Mineralogy of subducted basaltic crust (MORB) from
452 25 to 37 GPa, and chemical heterogeneity of the lower mantle. *Earth and Planetary*
453 *Science Letters*, 190: 57-63.
- 454 Ono, S. et al., 2002. Equation of state of Al-bearing stishovite to 40 GPa at 300 K. *American*
455 *Mineralogist*, 87(10): 1486-1489.
- 456 Schultz, E. et al., 2005. Double-sided laser heating system for in situ high pressure-high
457 temperature monochromatic x-ray diffraction at the ESRF. *High Pressure Research*,
458 25(1): 71-83.
- 459 Smyth, J.R., Swope, R.J. and Pawley, A.R., 1995. H in Rutile-Type Compounds .2. Crystal-
460 Chemistry of Al Substitution in H-Bearing Stishovite. *American Mineralogist*, 80(5-
461 6): 454-456.
- 462 Tsuchida, Y. and Yagi, T., 1989. A new, post-stishovite high-pressure polymorph of silica.
463 *Nature*, 340: 217-220.
- 464 van der Hilst, R.D., Widiyantoro, S. and Engdahl, E.R., 1997. Evidence for deep mantle
465 circulation from global tomography. *Nature*, 386: 578-584.
- 466
467

Table 1. Experimental run conditions and elastic parameters results

Run number	Pressure range* (GPa)	Laser used	Pressure medium and standard	Starting material	Vo measured (\AA^3)	Vo fitted using Eos (\AA^3)	Ko (GPa)	Method	Al content (p.f.u.) ³
Alsti-01	21.7 -> 10^{-4}	CO ₂	Ar	glass	46.861	46.866 (025) ¹ 46.875 (028) ²	284 ± 4 ¹ 278 ± 4 ²	Decompression	2.4
Alsti-07	15.2 -> 10^{-4}	CO ₂	Ar	glass	46.845	46.871 (020) ¹ 46.874 (022) ²	291 ± 5 ¹ 287 ± 5 ²		2.2
Alsti-06	43.5 -> 10^{-4}	CO ₂	Ar	glass	47.773	47.881 (049) ¹ 47.932 (060) ²	259 ± 3 ¹ 248 ± 4 ²		3.5
PV20	26.2 -> 99	YAG	NaCl + Pt	gel	-	46.513 (126) ¹ 46.770 (135) ²	322 ± 7 ¹ 292 ± 7 ²	Compression + annealing	
PV21	51.8 -> 10^{-4}	YAG	Ar + Pt	gel	47.043	47.076 (049) ¹ 47.121 (046) ²	300 ± 4 ¹ 287 ± 4 ²	Decompression	3.6
AlSti2	21 -> 49	YAG	Ar + Pt	gel	-			In-situ high temperature experiments	
AlSti5	19 -> 31	YAG	NaCl + Pt	gel	46.911				2.5
StiAl-01	23 GPa	YAG	NaCl + Pt	gel	46.983			In-situ high temperature experiments	3.1
StiAl-02	26 GPa	YAG	NaCl + Pt	gel	-				
StiAl-03	36 GPa	YAG	NaCl + Pt	gel	47.055				3.7

* pressure measured by the Pt or Ar scale (Jamieson et al., 1982; Jephcoat, 1998).

¹ elastic parameters fitted using a second order Birch-Murnaghan eos using a K' of 4, and

² K' of 4.59 as in the case of pure SiO₂ (Andrault et al., 2003). Pressure for determining the Eos is measured thanks to Pt or Ar Eos (Holmes et al., 1989; Jamieson et al., 1982; Jephcoat, 1998).

³ as determined from **Figure 5**.

- Andrault, D., Angel, R.J., Mosenfelder, J.L. and Le Bihan, T., 2003. Equation of state of the stishovite to lower mantle pressures. *American Mineralogist*, 88: 301-307.
- Holmes, N.C., Moriarty, J.A., Gathers, G.R. and Nellis, W.J., 1989. Equations of state of platinum to 660 GPa (6.6 Mbar). *Journal of Applied Physics*, 66: 2962-2967.
- Jamieson, J.C., Fritz, J.N. and Manghnani, M.H., 1982. Pressure measurement at high temperature in x-ray diffraction studies: gold as a primary standard. In: S. Akimoto and M.H. Manghnani (Editors), *High Pressure Research in Geophysics*. Riedel, Boston, pp. 27-48.
- Jephcoat, A.P., 1998. Rare-gas solids in the Earth's deep interior. *Nature*, 393: 355-358.

Accepted Manuscript

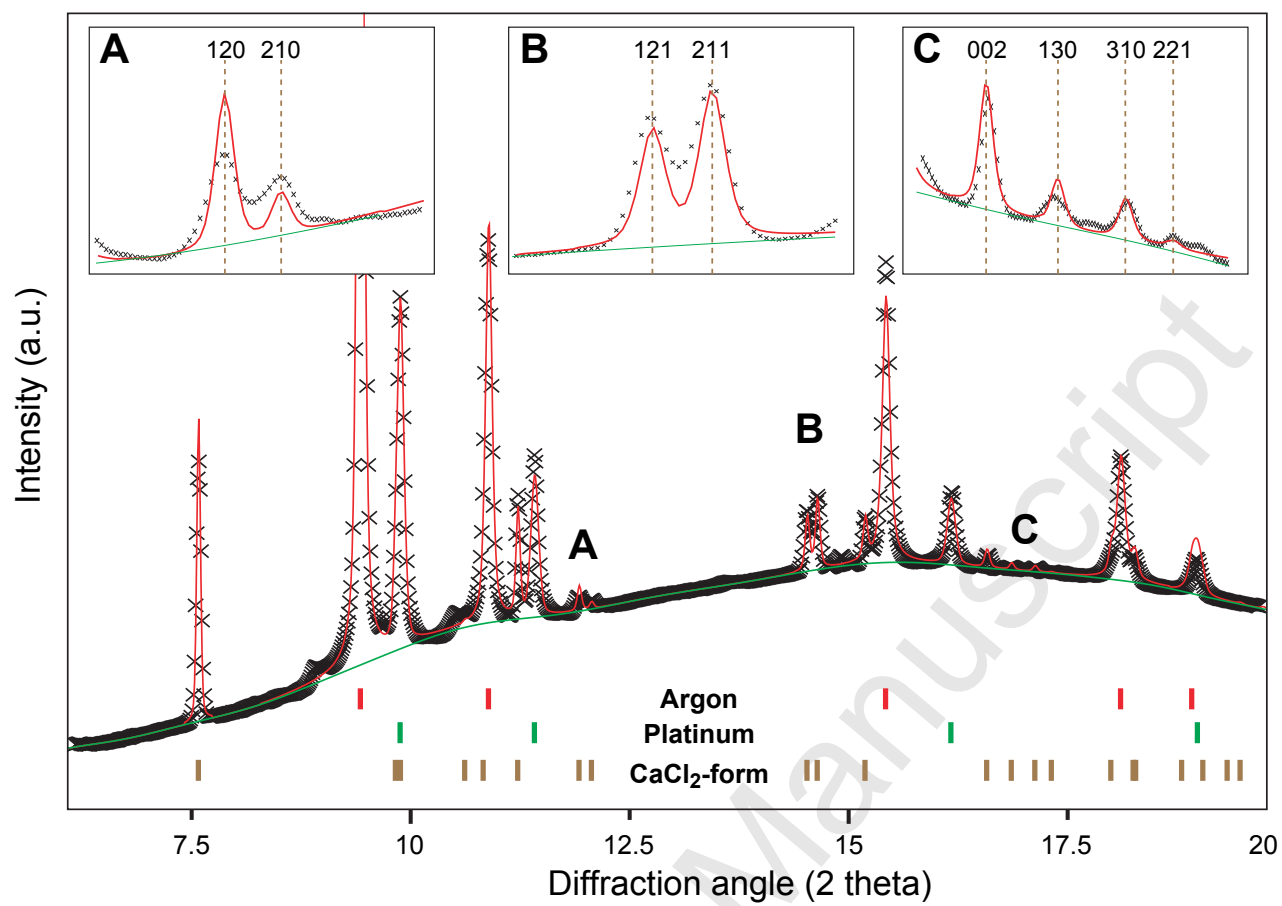


Figure 1

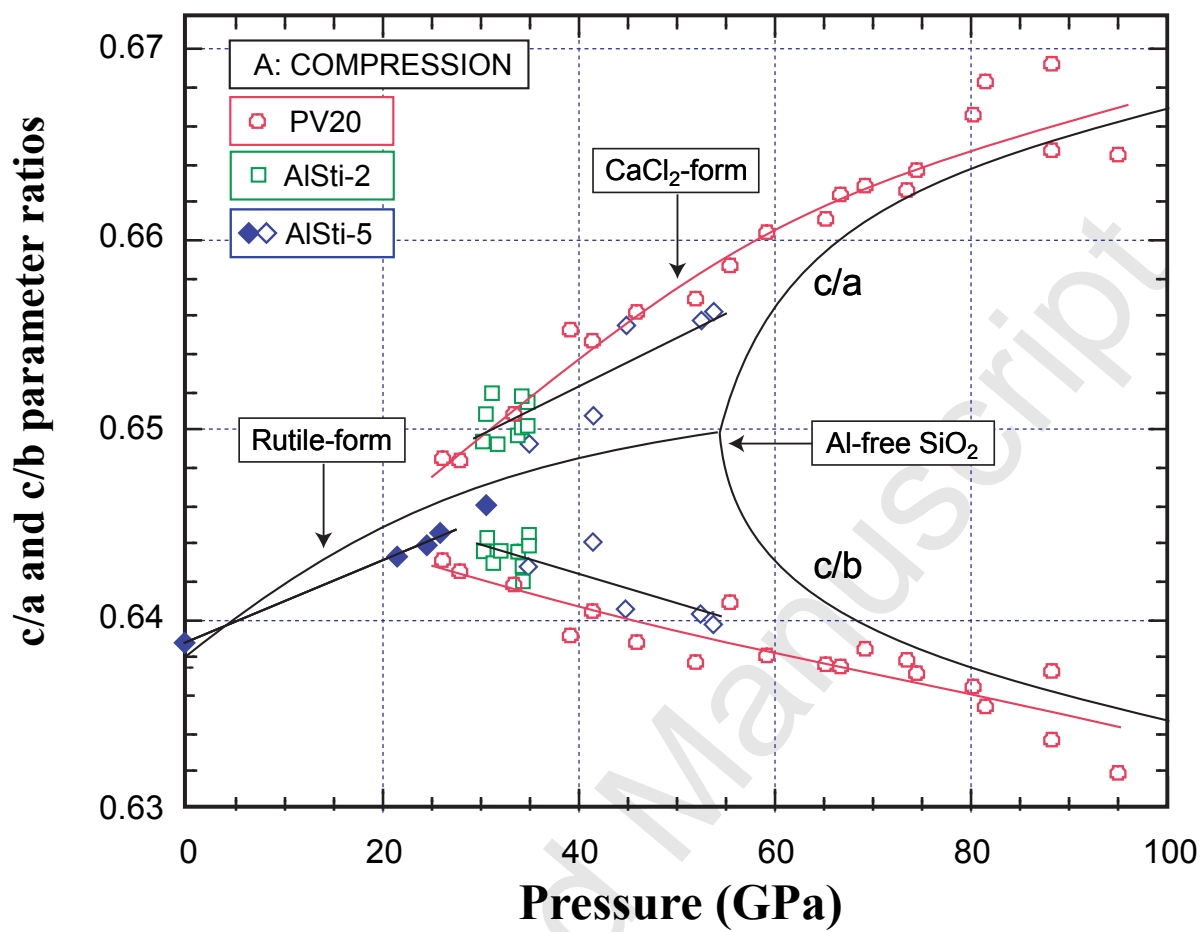


Figure 2a

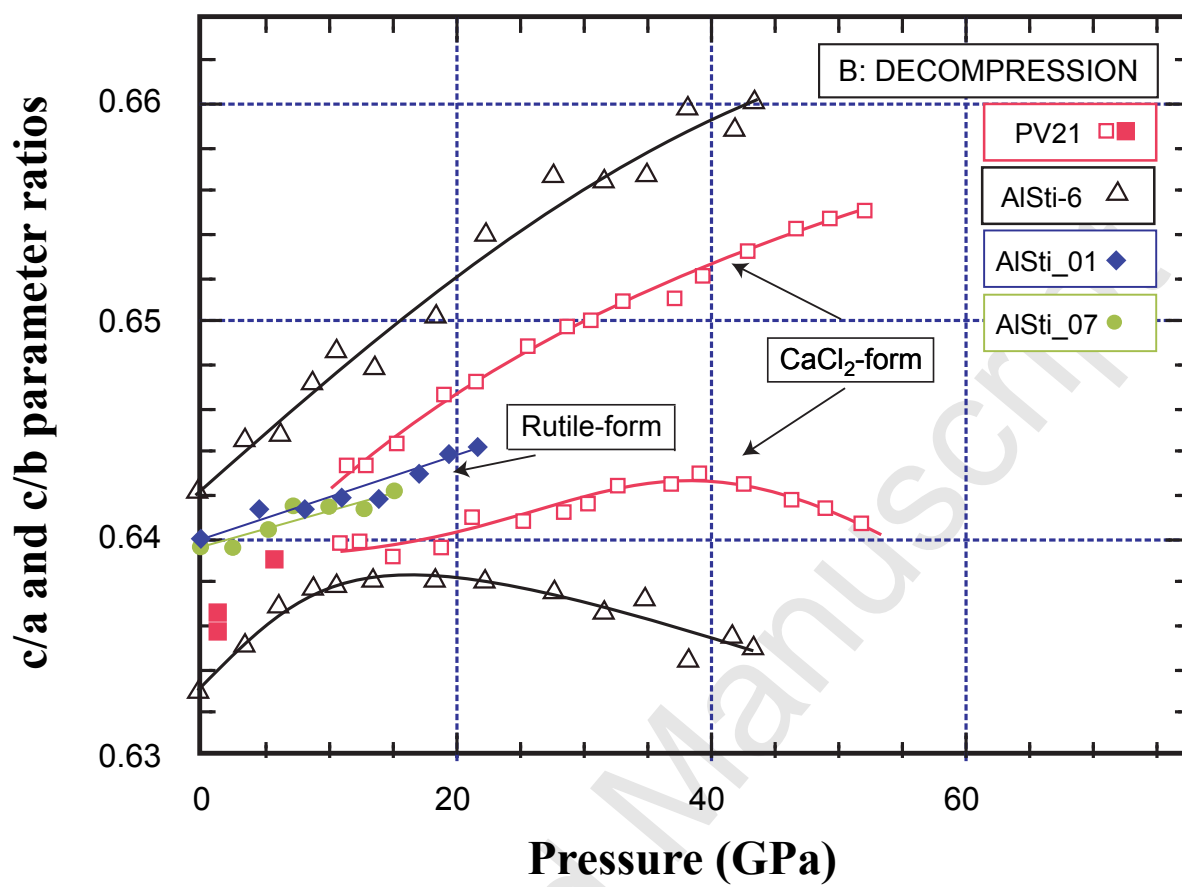


Figure 2b

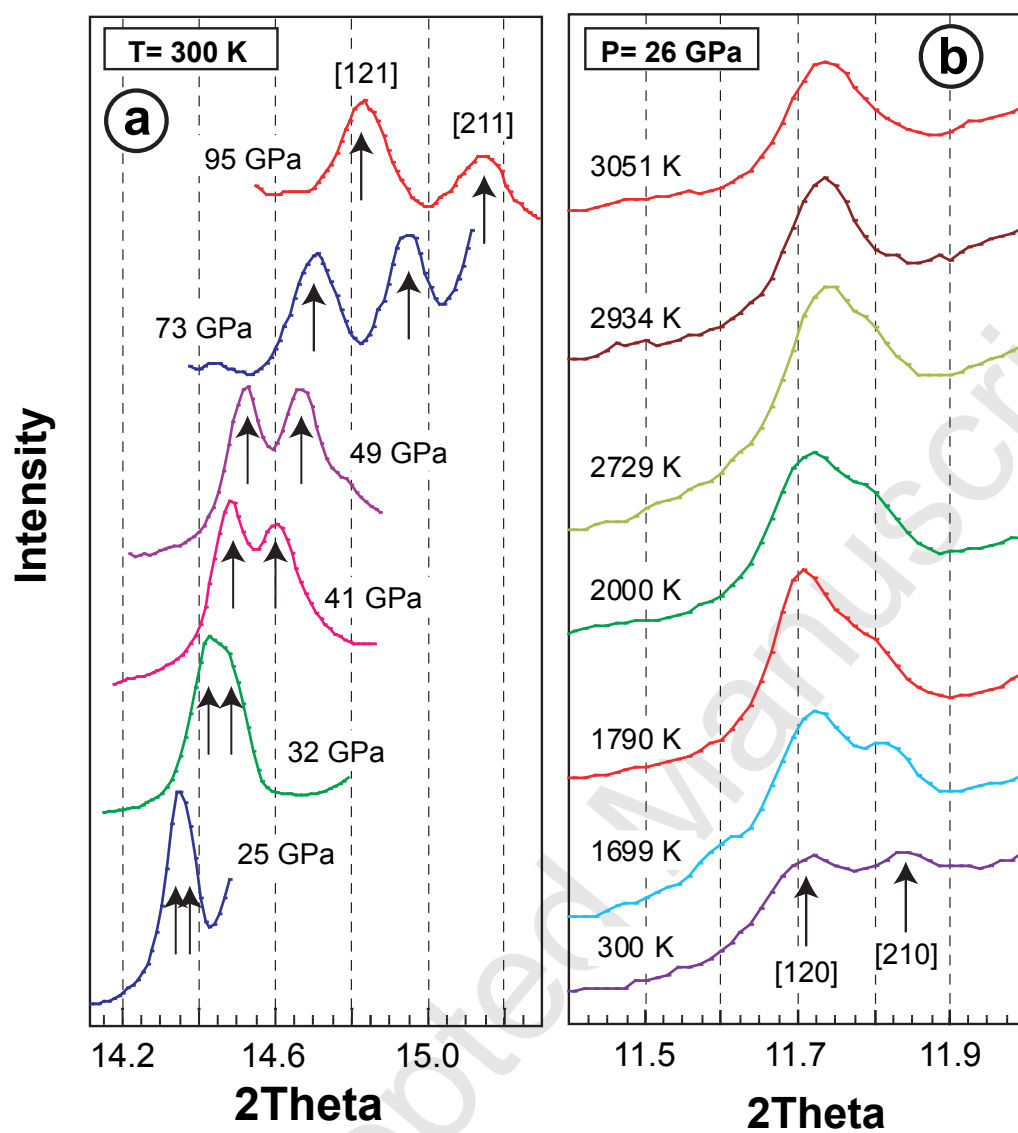


Figure 3

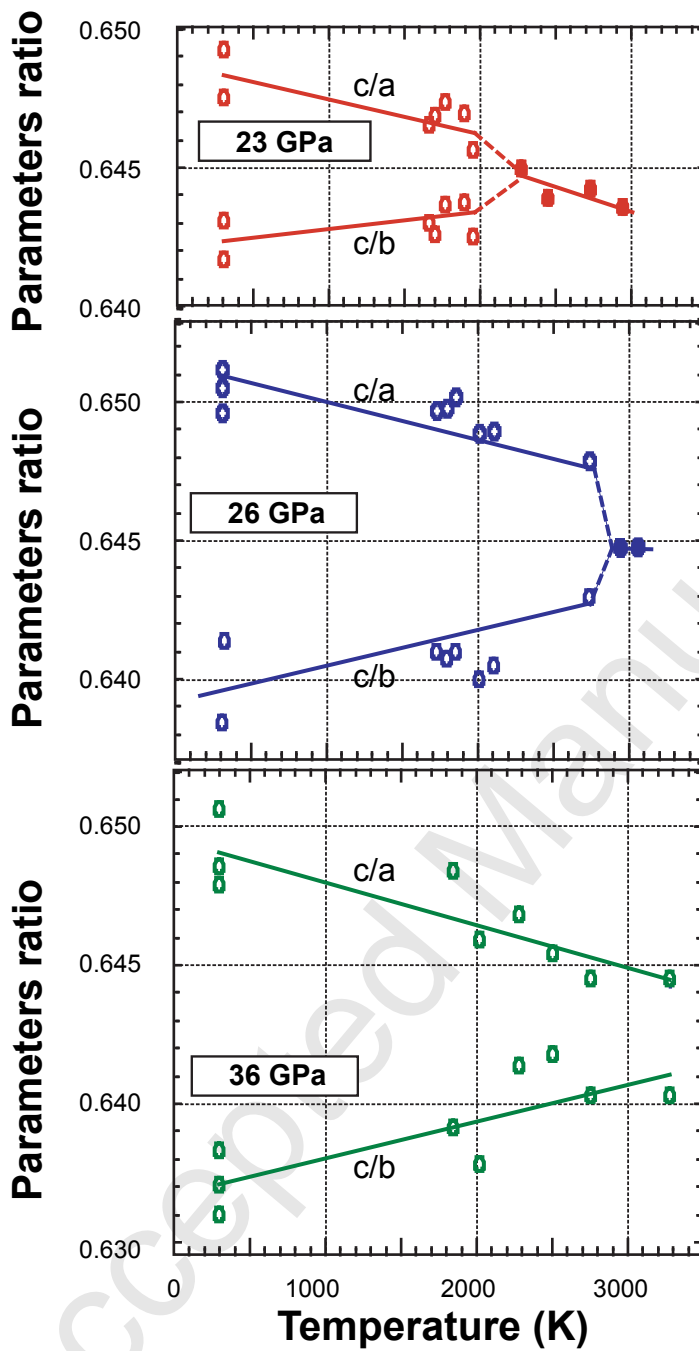


Figure 4
Page 26 of 31

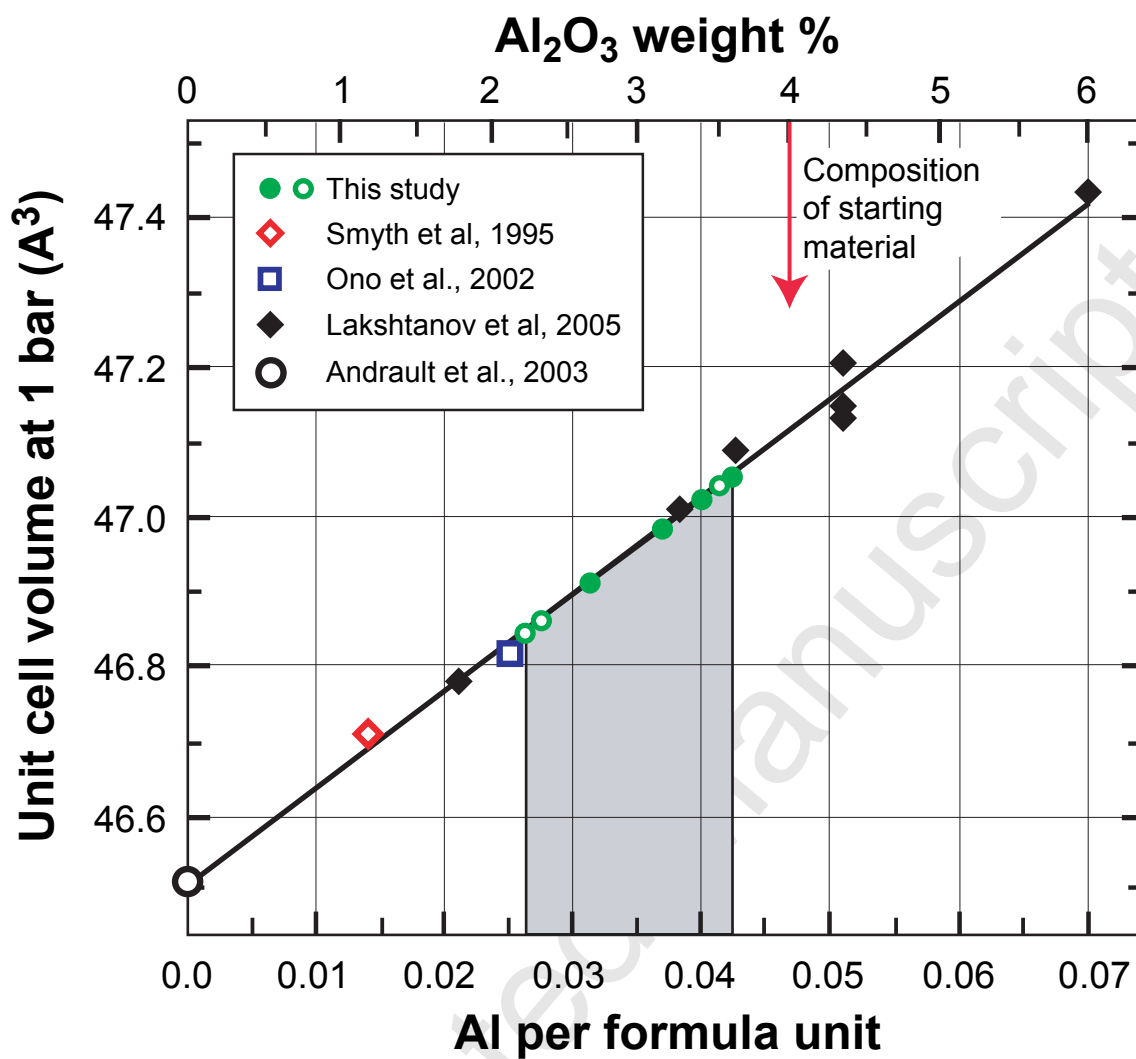


Figure 5

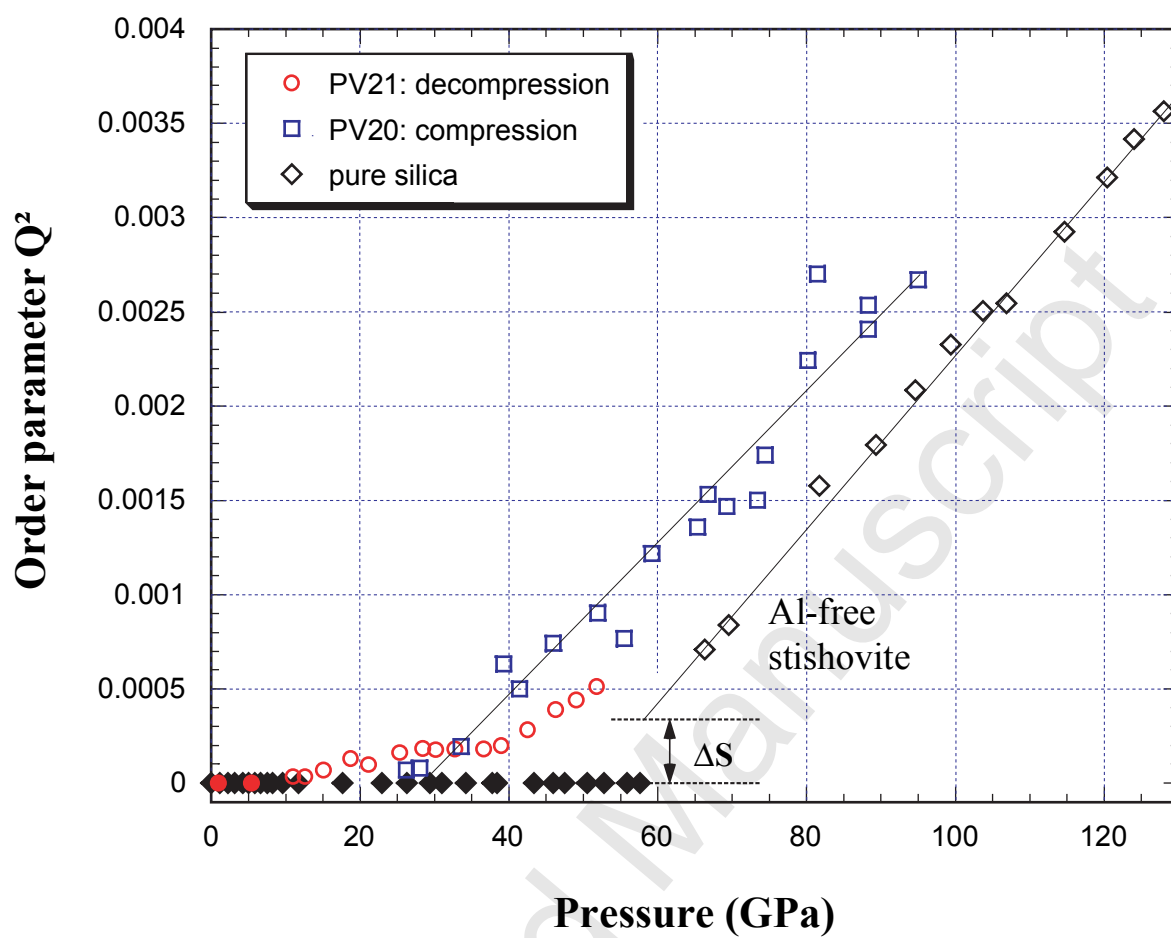


Figure 6

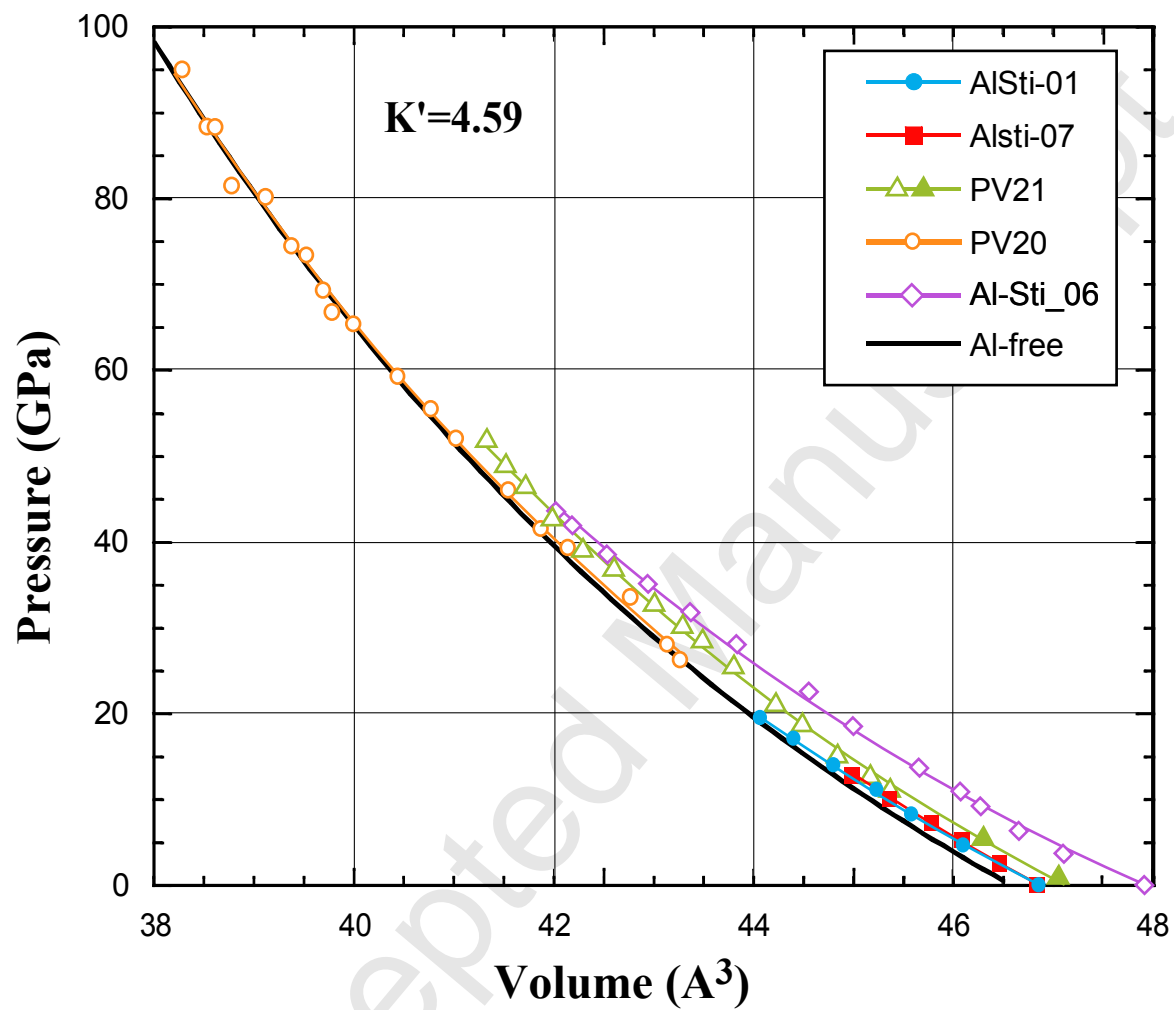


Figure 7

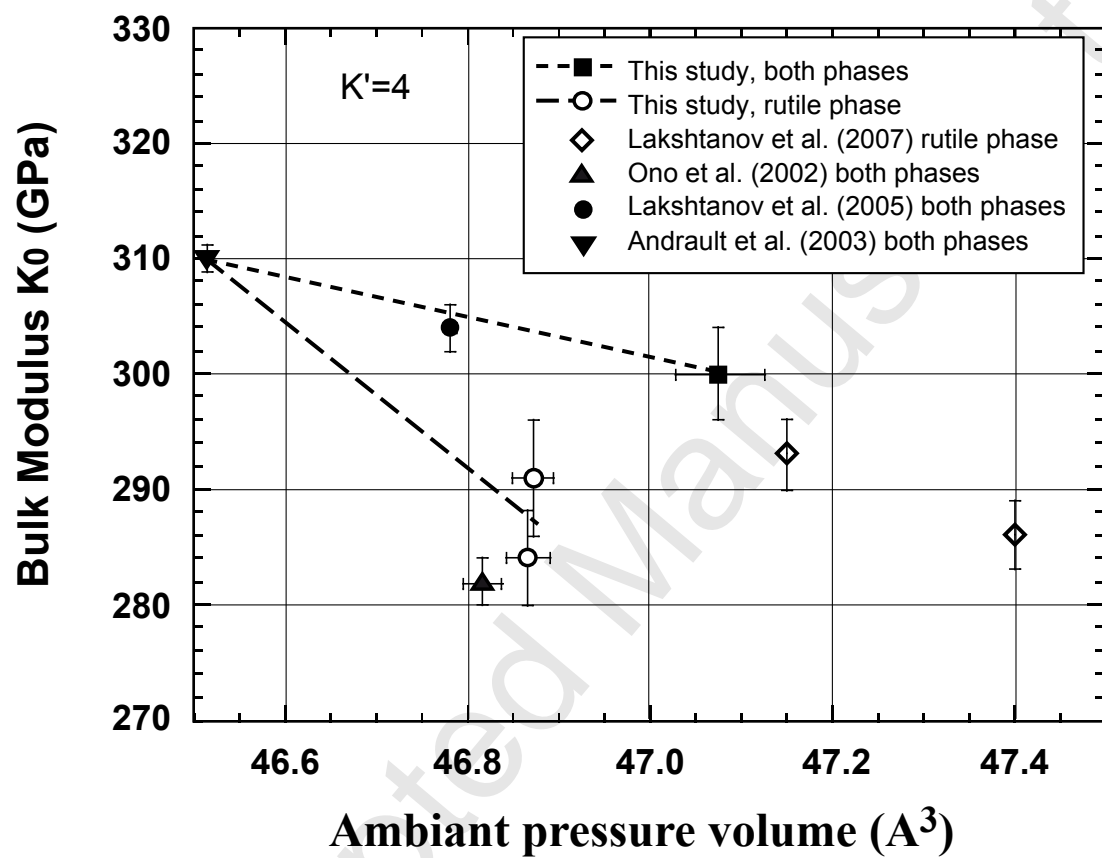


Figure 8

